METEOR SHOWER FORECASTING FOR SPACECRAFT OPERATIONS

Althea V. Moorhead[(1)], William J. Cooke[(1)], and Margaret D. Campbell-Brown[(2)]

[(1)]*NASA Meteoroid Environment Office, Marshall Space Flight Center, Huntsville, Alabama 35812, Email: {althea.moorhead, william.j.cooke}@nasa.gov*
[(2)]*Department of Physics and Astronomy, The University of Western Ontario, London N6A3K7, Canada, Email: margaret.campbell@uwo.ca*

ABSTRACT

Although sporadic meteoroids generally pose a much greater hazard to spacecraft than shower meteoroids, meteor showers can significantly increase the risk of damage over short time periods. Because showers are brief, it is sometimes possible to mitigate the risk operationally, which requires accurate predictions of shower activity. NASA's Meteoroid Environment Office (MEO) generates an annual meteor shower forecast that describes the variations in the near-Earth meteoroid flux produced by meteor showers, and presents the shower flux both in absolute terms and relative to the sporadic flux. The shower forecast incorporates model predictions of annual variations in shower activity and quotes fluxes to several limiting particle kinetic energies. In this work, we describe our forecasting methods and present recent improvements to the temporal profiles based on flux measurements from the Canadian Meteor Orbit Radar (CMOR).

Key words: meteoroids.

1. INTRODUCTION

Meteoroid impacts are known to cause damage to spacecraft surfaces; their high speed (12-72 km s^{-1}) compared to orbital debris means that relatively small particles can be hazardous. Most of the meteoroid flux is associated with "sporadic" meteoroids, which are those not associated with any meteor shower. The sporadic complex is present throughout the year and constitutes the vast majority of microgram-or-larger meteoroids. For this reason, meteoroid environment models such as NASA's Meteoroid Engineering Model (MEM) [1, 2] and ESA's Interplanetary Meteoroid Environment Model (IMEM) [3] focus on the sporadic complex. Although these models include showers in the total meteoroid flux, they do not model the short-duration fluctuations caused by showers. Such fluctuations are generally not worth modeling for a long-duration spacecraft mission.

Over short time spans, however, meteor showers can match or even exceed the sporadic flux. The Geminid meteor shower, for example, can double the meteoroid flux at the time of peak activity. The Leonid meteor shower does not pose much of an impact risk on a typical year, but has occasionally produced outbursts in which the number of meteors is tens to thousands of times larger than normal [4]. In such cases, operational spacecraft sometimes choose to mitigate the risk by avoiding operations that increase the spacecraft's vulnerability. If the risk is great enough, operators may consider re-orienting the spacecraft to present its least vulnerable side to the shower, phasing its orbit to use the Earth as a shield, or powering down components.

All mitigation strategies have some associated cost such as delays, reduced functionality, or fuel. Accurate shower predictions are therefore needed for informed risk assessment. The Meteoroid Environment Office (MEO) produces annual meteor shower forecasts that can be used to assess the increase in the particle flux due to showers. These forecasts are designed to be used in conjunction with an existing sporadic meteoroid risk assessment; unlike sporadic models, however, the annual forecast provides a detailed temporal profile that takes showers into account. The forecast also takes shower variability into account; any unusual activity predicted by modelers [5, 6] is incorporated.

While modelers can often predict the level of meteor shower activity, we frequently rely on past observations to characterize the activity *profile*. For many years, the MEO (and others; [7]) used a set of activity profiles that were determined from naked-eye meteor observations [8]. Many of the activity profiles in this set are quite noisy due to low number statistics. Furthermore, daytime meteor showers were of course not visible to observers and thus the MEO had to employ a default activity profile for many of these showers.

Meanwhile, the Canadian Meteor Orbit Radar (CMOR) began operation in 2001 [9]. CMOR is a patrol radar and can detect meteor echoes during the day as well as at night. It is located near London, Ontario and thus monitors the northern hemisphere, although it can detect meteors with declinations as low as -40°. Meteor flux measurements from CMOR [10] are available for the years 2002-2015, providing us with a data set suitable for re-

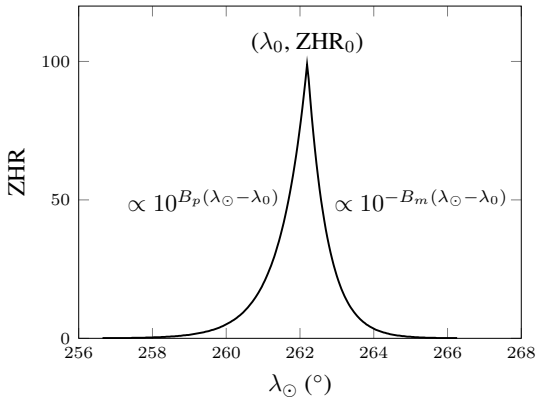

Figure 1. Sample meteor shower activity profile. The peak zenithal hourly rate is ZHR_0 *and the peak occurs at solar longitude* λ_0*. On either side the activity follows an exponential function of solar longitude; the two parameters* B_p *and* B_m *are not necessarily equal.*

vising many shower activity profiles.

This paper presents both our methodology for shower forecasting (Section 2) and the improvements we've made to our shower activity profiles based on CMOR flux measurements (Section 3). Finally, Section 4 discusses the forecast and the changes in it from a spacecraft risk perspective.

2. FORECASTING METHODS

This section describes our algorithm for forecasting meteor shower fluxes. These fluxes are derived from a set of meteor shower parameters and are adjusted for an altitude of 400 km. We also compute the appropriate sporadic meteor flux at this altitude, taking gravitational focusing and planetary shielding into account. Finally, we compute the flux enhancement produced by these showers over the baseline meteoroid flux.

2.1. Shower fluxes

Meteor showers do not have a well-defined duration. Instead, peak activity occurs at a particular time each year and activity gradually increases up to the peak and decreases after the peak (see Fig. 1). A double exponential function has been found to be a good fit to most meteor shower activity profiles [8]. Measures of effective shower duration (such as the full width at half maximum or time period over which activity exceeds a given threshold) thus depend on the steepness of this double exponential function.

We characterize the activity profile of each shower with four parameters: peak time (λ_0), peak zenithal hourly rate (ZHR_0), and two exponents that characterize the shape of the shower's activity profile (B_p and B_m). The time of peak shower activity occurs when the center of the meteoroid stream intersects the Earth's orbit; we therefore measure time in terms of solar longitude, $\lambda_\odot$. The zenithal hourly rate (ZHR; the rate at which meteors occur when the shower radiant is directly overhead) increases with time before the peak and decreases after the peak:

$$\mathrm{ZHR} = \mathrm{ZHR}_0 \cdot \begin{cases} 10^{+B_p(\lambda_\odot - \lambda_0)} & \lambda_\odot < \lambda_0 \\ 10^{-B_m(\lambda_\odot - \lambda_0)} & \lambda_\odot > \lambda_0 \end{cases} \quad (1)$$

In some cases, such as the Perseids, the activity profile of a single meteor shower is constructed from two sets of parameters that describe "peak" and "base" activity.

ZHR describes the rate at which a meteor shower produces visible meteors. ZHR can be converted to meteor flux by taking into account observer biases and shower characteristics. We use the methodology of [11] to calculate the flux of meteoroids that have a brightness of at least magnitude 6.5:

$$f_{6.5} = \frac{\mathrm{ZHR}_0 \cdot k_{\mathrm{avg}} \cdot (13.1r - 16.5)(r - 1.3)^{0.748}}{37200 \text{ km}^2} \quad (2)$$

where the average perception factor, k_{avg}, is of order unity. The population index, r, describes the brightness distribution of meteors within the shower and is also required as an input for each shower. Because ZHR has units of hr^{-1}, this equation yields flux in units of km^{-2} hr^{-1}.

This magnitude-limited flux can be converted to a mass-limited (milligram or larger) flux as follows [11]:

$$f_{\mathrm{mg}} = f_{6.5} \cdot r^{9.775 \log_{10}\left(29 \text{ km s}^{-1} / v_{100}\right)} \quad (3)$$

This equation makes use of Verniani's relationship [12] between magnitude, mass, and velocity to calculate the meteoroid mass that produces a magnitude 6.5 meteor at the shower's speed. The shower velocity is that at the top of the atmosphere.

Finally, the flux can be scaled to any arbitrary limiting mass using the relation:

$$\frac{f_m}{f_{\mathrm{mg}}} = \left(\frac{m}{1 \text{ mg}}\right)^{1-s} \quad (4)$$

where $s = 1 + 2.3 \log_{10} r$ is the shower mass index.

In all annual meteor shower forecasts to date, an additional factor of 2 was applied to Eq. 2. This factor was obtained by applying Eq. 2 to the Grün interplanetary flux [13] and comparing it with a sporadic ZHR estimate of 8. A factor of 2 was found to bring them in rough agreement. However, a separate mass-luminosity relationship was used to convert magnitude to mass in that calculation. When Eq. 3 is used instead, the flux corresponding to a sporadic ZHR is a factor of 4 larger, obviating the

Table 1. The four kinetic energies (KE_{ref}) to which the MEO annual meteor shower forecast reports fluxes. The second column lists the particle mass which, at 20 km s^{-1}, has the listed kinetic energy. The third column lists the particle diameter which, for a bulk density of 1000 kg m^{-3}, has the listed mass.

KE_{ref} (J)	m_{ref} (g)	d_{ref} (cm)
6.7	3.35×10^{-5}	0.04
104.7	5.24×10^{-4}	0.1
2827.	1.41×10^{-2}	0.3
104720.	5.24×10^{-1}	1.0

need for a factor of 2. Additionally, the meteoroid speed distribution [1, 14, 15] is much broader than the Grün assumption of a constant 20 km s^{-1}. When we fold a speed *distribution* through Eq. 2, we obtain a number that can differ from that obtained using a single speed of 20 km s^{-1} by a factor of 2. Finally, the ZHR of ~ 8 that was used for this calibration may originate from [8] and is thus based on an *hourly* rate (HR), not ZHR. A later sporadic ZHR estimate by Rendtel took sporadic source radiants into account and yielded ZHR~ 22 for the apex source alone.[16, 17] For these reasons, we conclude that the sporadic ZHR does not present a robust calibration point for Eq. 2 and therefore drop the factor of 2 that was previously applied.

Most ballistic limit equations (BLEs) are proportional or near-proportional to kinetic energy, not mass [18]. Therefore, the MEO shower forecast quotes fluxes corresponding to four characteristic kinetic energies, listed in Table 1. Put another way, shower fluxes are calculated for four limiting meteoroid masses which relate to our reference masses in the following way:

$$m_{\text{lim}} = m_{\text{ref}} \times \left(\frac{20 \text{ km s}^{-1}}{v_{400}} \right)^2 \tag{5}$$

where v_{400} is the shower's speed at an altitude of 400 km.

Historically, the meteor shower forecast has applied an "obscuration factor" of 0.6 (corresponding to an altitude of 400 km) to each shower flux to account for the fact that the Earth can, at times, shield the spacecraft from the shower. We omit this term from future forecasts for two reasons. First, this shielding effect is velocity-dependent [19], and therefore a constant value of 0.6, while close to the correct values, is not strictly correct. Second, it is important to provide spacecraft operators with a "worst-case scenario;" such a scenario would involve full exposure to the meteoroid stream at the time of peak activity. (This obscuration factor did largely negate the factor of 2 that was previously applied to Eq. 2, resulting in shower fluxes that were over-conservative by only 20%.)

We do include gravitational focusing, wherein the flux of slow showers in particular is increased at the top of the atmosphere due to Earth's gravitational pull. Because shower fluxes are measured at the top of the atmosphere, we must invert the gravitational focusing effect to obtain the slightly lower shower flux corresponding to an altitude of 400 km [19]:

$$\frac{f_{400}}{f_{100}} = \left(\frac{v_{400}}{v_{100}} \right)^2 \tag{6}$$

This effect is small: we find that for our slowest shower (the Draconids, at 20 km s^{-1}), the flux at 400 km altitude is 98.6% of the flux at 100 km altitude. This difference is within our uncertainties but we include it for the sake of completeness.

In addition to computing fluxes, the meteor shower forecast code integrates each flux to calculate the meteoroid fluence over a given time interval. This time interval is either the default value of 7 hours or an interval requested by a customer.

2.2. Sporadic flux

In order to facilitate risk assessments, the meteor shower forecast compares the total shower flux at a given time with the total time-averaged meteoroid flux. The total time-averaged flux includes both shower and sporadic meteoroids; as a result, periods of low shower activity correspond to a *reduction* in risk, while periods of high shower activity correspond to an *increase* in risk.

The total meteoroid flux in interplanetary space is calculated using Eq. A3 of [13], which was derived assuming an interplanetary meteoroid speed distribution with $v_{\text{rms}} = 20$ km s^{-1}. An interplanetary speed of 20 km s^{-1} corresponds to a speed of 22.75 km s^{-1} at a location 400 km above the Earth's surface. We therefore calculate four reference sporadic masses using Eq. 5 and $v_{400\text{ km}} = 22.75$ km s^{-1}.

We convert the Grün interplanetary flux to one valid at 400 km altitude by taking gravitational focusing and planetary shielding into account. The enhancement of the interplanetary flux caused by gravitational focusing is given by [19]:

$$\eta_{\text{g}} = \frac{v_{400}^2}{v_{\text{IP}}^2} \tag{7}$$

where $v_{400} = 22.75$ km s^{-1} is the speed at 400 km and $v_{\text{IP}} = 20$ km s^{-1} is the interplanetary meteoroid speed. The fraction of the interplanetary flux that remains after planetary shielding is given by:

$$\sin\psi = \frac{v}{v_x} \cdot \frac{R_\oplus + 100 \text{ km}}{R_\oplus + 400 \text{ km}} \tag{8}$$

$$\eta_{\text{s}} = \frac{1 + \cos\psi}{2} \tag{9}$$

where v is meteoroid speed at the top of the atmosphere and $R_\oplus = 6371$ km is the radius of the Earth.

The resulting sporadic fluxes for our chosen altitude of 400 km range from 4.18×10^{-2} m^{-2} yr^{-1} for our smallest particle energy to 1.93×10^{-7} m^{-2} yr^{-1} for our largest particle energy.

Previous versions of the shower forecast used Eqns. 7-5 and 7-6 of [20] to compute the gravitational focusing and shielding at 400 km. However, Eq. 7-6 is not correct for a interplanetary meteoroid speed of 20 km s^{-1}, nor is it correct for the speed distribution presented in [20]. Additionally, the forecast previously did not use the 22.75 km s^{-1} speed at 400 km to adjust the reference masses; once again, these two choices fortuitously had opposite effects, resulting in a baseline flux that was close to accurate.

2.3. Enhancement factors

Finally, the meteor shower forecast reports flux enhancement factors, which quantify the increase in flux produced by showers over the baseline Grün flux. We assume that the Grün flux includes showers, but is time-averaged, while the shower flux varies with time. Additionally, Grün's flux equation [13] reports the meteoroid flux incident on a randomly tumbling flat plate in interplanetary space. The shower fluxes discussed in Section 2.1 represent those on a plate facing the shower radiant; the zenithal hourly rate applies when the radiant is directly above the collecting surface. This combination produces a worst-case scenario shower-to-sporadic flux ratio, in which the spacecraft surface faces the meteor shower and does not benefit from planetary shielding.

Both the orientation requirement and lack of shielding must be discarded, however, in order to calculate the *average* shower contribution to the total meteoroid flux. Let us assume that the Grün flux (f_{G}) consists of a sporadic background flux (f_{b}) plus a time- and direction-averaged shower flux (f_{s}). The intercepted shower flux is proportional to $\cos\theta$, where θ is the angle between a surface's normal vector and the shower radiant. If we average $\cos\theta$ over all directions, and compare to the flux intercepted when $\theta = 0$, we obtain the following ratio:

$$\frac{\int_0^{2\pi}\int_0^{\pi/2}\cos\theta\sin\theta\,d\theta\,d\phi}{\int_0^{2\pi}\int_0^{\pi}\sin\theta\,d\theta\,d\phi} = \frac{1}{4}\,. \qquad (10)$$

If we also include the reduction in flux produced by planetary shielding (η_{s}), the fraction of the Grün flux made up of shower meteors is $\alpha = f_{\mathrm{s}}/f_{\mathrm{G}} = \frac{1}{4}\langle f_{400}(\lambda_\odot)\eta_{\mathrm{s}}\rangle/f_{\mathrm{G}}$, if f_{400} represents the shower flux on an un-shielded plate facing the shower radiant at 400 km altitude. This in turn allows us to calculate the sporadic flux as $f_{\mathrm{b}} = (1-\alpha)f_{\mathrm{G}}$.

Finally, the fractional enhancement of the flux due to showers at any point in time is:

$$g = \frac{f_{400}(\lambda_\odot) + f_{\mathrm{b}} - f_{\mathrm{G}}}{f_{\mathrm{G}}} = \frac{f_{400}(\lambda_\odot) - \alpha f_{\mathrm{G}}}{f_{\mathrm{G}}}\,. \qquad (11)$$

The forecast reports this enhancement factor as a percentage of the Grün flux. Note that we use f_{400}, rather than $\frac{1}{4}f_{400}\eta_{\mathrm{s}}$, to calculate g. The enhancement factors therefore reflect the increase in meteoroid flux on an unshielded plate facing the shower radiant, which is in keeping with our goal of providing worst-case shower fluxes.

We calculate α using a set of standard meteor shower parameters that represent shower activity in a "typical" year. However, in any given year, individual showers could exceed or fall short of the standard, in which case $\frac{1}{4}\langle f_{400}(\lambda_\odot)\eta_{\mathrm{s}}\rangle/f_{\mathrm{G}} \neq \alpha$.

The meteor shower forecast reports the total shower enhancement as a function of time, taking all active showers into account. Our g is thus technically an overestimate, as a flat surface cannot be normal to multiple radiants at once. However, one shower usually dominates at any given time and g therefore remains a useful estimate of the increase in meteoroid flux. The meteor shower forecast also provides radiant information for the most significant showers. If the flux enhancement exceeds a mission's risk tolerance, the forecast fluxes can be used in combination with these radiants to refine the meteoroid impact risk assessment.

The meteor shower forecast has historically assumed that the Gr un flux contains both sporadic and shower meteors [13]. This choice was made based on personal communication with the authors of that work, who claimed to have made no attempt to separate the two types of meteors. We plan to revisit this assumption in the future and determine whether the Grün flux equation is consistent with or exceeds sporadic-only flux measurements.

3. FLUX MEASUREMENTS AND ACTIVITY PROFILES

The lists of shower inputs used to generate MEO meteor shower forecasts are derived from a variety of sources. The shape parameters (λ_0, B_p, and B_m) for most showers are taken from [8], who fit double-exponential activity curves to visual observations of meteor showers. His data were provided by observers in both the northern and southern hemispheres. However, visual observers are not able to measure rates for daytime showers unless they occur near dawn or dusk, and are in general less able to measure radiants accurately.

In this work, we use 14 years of CMOR fluxes to revise our meteor shower activity profiles. These fluxes are single station, but the sporadic contamination has been substantially reduced by placing a detection angle restriction on meteor detections. Radar detection of a meteor requires that the meteor trail be perpendicular to the line-of-sight. As a result, meteors associated with a particular radiant are detected along a great circle that lies in a plane perpendicular to that radiant. Selecting only those meteors that lie along this great circle removes a large number of sporadic meteors but preserves shower meteors. When multiple showers are active, these circles can intersect; such points of intersection have been excluded. Despite these measures, some background contamination persists, which we remove in Section 3.1.

CMOR's gain pattern and radiant coverage have been taken into account to compute fluxes; see [10] for addi-

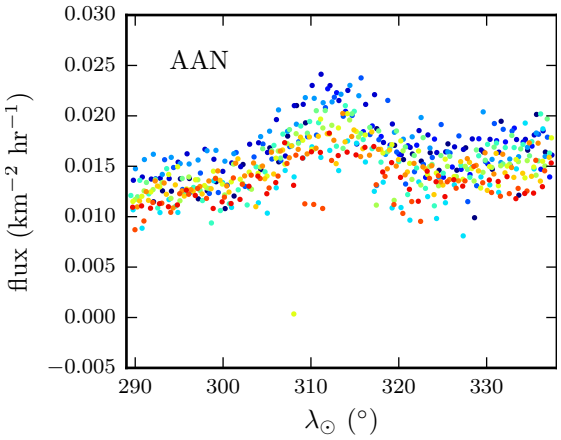

Figure 2. Raw fluxes corresponding to the AAN radiant measured by CMOR. The data are color-coded by year, where early years are blue and later years are red. Note the single, light-green outlier with a flux of nearly zero.

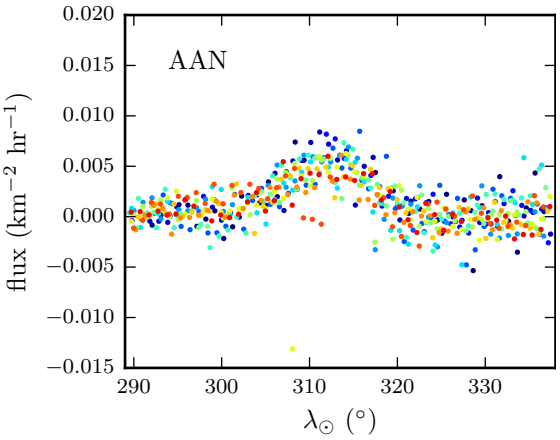

Figure 3. Detrended fluxes corresponding to the AAN radiant measured by CMOR. The data are color-coded by year, where early years are blue and later years are red.

tional details. Some uncertainty remains regarding the magnitude of these fluxes, but relative fluxes are thought to be robust and appropriate for constraining the shape, if not the peak value, of shower activity profiles.

CMOR provides average fluxes for one-day intervals, and so a single year of data cannot provide a tight constraint on the exact peak time of the shower. However, the solar longitude corresponding to a given day varies by year, and so by combining many years of data, we can in some cases measure the peak time with less than 1-day resolution.

3.1. Detrending

Fig. 2 shows the raw flux over all years for an example shower: the α Antliids (AAN). Several issues with the data are apparent: [1] the shower appears as an enhancement over the background flux, [2] the background flux appears to contain a trend with solar longitude, [3] the background flux tends to decrease over the years, and [4] anomalous outliers are present in the measurements.

Our first task is to characterize and remove the background flux, to which we fit a simple linear trend. In order to minimize the shower's influence on this fit, we apply the following weights, w to the data:

$$w = (\lambda_\odot - \lambda_{\text{nom}})^2 \tag{12}$$

where $\lambda_\odot$ is solar longitude and λ_{nom} is the solar longitude corresponding to an estimate of the peak time. We then subtract this linear trend from the data. We find that this simple approach works fairly well to remove most of the background flux and nullify trends within it.

We refine our removal of the background flux by fitting for an offset between the average background flux and the background flux per year. In this case, we attempt to exclude the shower and outliers by obtaining the average flux for values between the 10th and 50th percentiles. Thus, if a shower spans more than half of the observation period, the background flux will be overestimated. Fig. 3 shows the result of our background removal approach.

3.2. Fitting

We next fit a double-exponential profile (see Eq. 1) to our detrended data using χ^2-minimization. We fit for the peak time, peak flux, and the two exponents governing the rise and decay of the shower (B+ and B-). Because CMOR measures flux over day-long periods, we also convolve this double-exponential profile over a one-day period before fitting it to the data. A fit to another example shower, the Daytime Sextantids (DSX), is shown in Fig. 4.

In our example as well as for a number of other showers, the shower amplitude appears to vary with year. This may be related to the decrease in the background over time. When this trend is apparent in a set of shower fluxes, we fit the amplitude of the double-exponential profile to each year's data. We then renormalize each year's data to the nominal amplitude and iterate our double-exponential fit. This produces a small refinement in our fit. The results are shown in Fig. 5.

In the example of the Daytime Sextantids, the data and our derived activity profile differ significantly from our previously used profile. In the next section, we summarize our data and implications for the annual forecast.

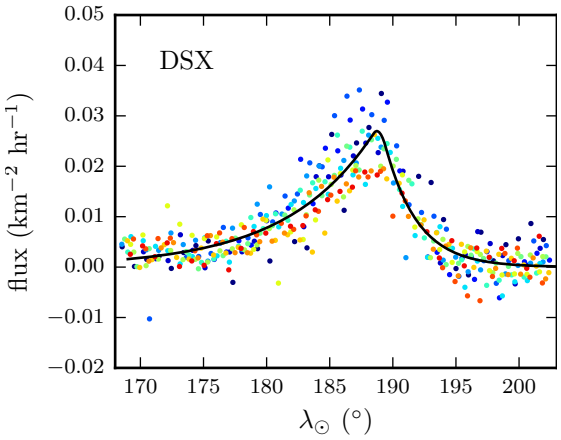

Figure 4. A double exponential activity profile (black line) fit to detrended fluxes (points) corresponding to the DSX radiant as measured by CMOR. After fitting is complete, we remove points that lie more than 5σ away from the fitted profile – in this case, five such outliers have been removed.

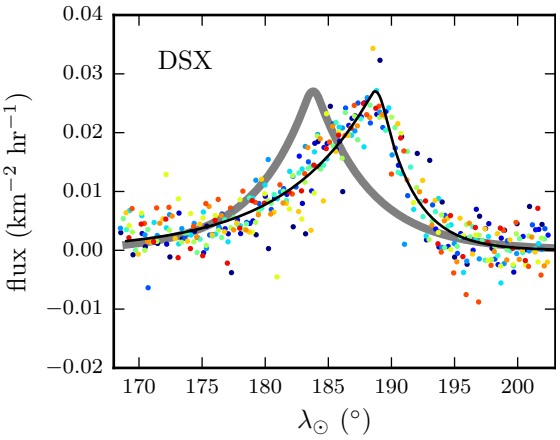

Figure 5. A double exponential activity profile (black line) fit to detrended fluxes (points) corresponding to the DSX radiant as measured by CMOR. The amplitude has been permitted to vary by year; in this plot, each year's data has been renormalized to match the average flux amplitude. The activity profile used in previous meteor shower forecasts (thick gray line) is included for the sake of comparison.

3.3. Revised list of showers

We were able to characterize the activity profiles for 12 major meteor showers using CMOR flux measurements. In some cases, such as the Orionids (ORI), our fitted parameters closely resembled those of [8]. In other cases, such as the Daytime Arietids, our activity profile parameters changed substantially. Table 2 shows the list of all updated showers, including previous and updated values of all parameters.

The updated showers include the Geminids (GEM); we altered the shape of this shower to be much broader. We made this choice because CMOR measures fluxes at particle sizes that are close to the limiting particles sizes for typical spacecraft risk assessments. However, the shape of the Geminid activity profile is believed vary with limiting particle size; we plan to incorporate this behavior into the forecast at a future date.

In many cases, we were unable to improve the activity profiles (see Table 3). Showers fell into this category for a variety of reasons: their activity may have been too low to be clearly detected by CMOR, they may have been located in the southern sky and out of CMOR's range (SSG), they may have had brief, inconsistent outbursts (DRA), or they may have had such an extended activity profile that we risked removing shower flux along with the background (NTA, STA, BTA). We hope to improve our characterization of many of these showers in the future using flux measurements from other sources.

Finally, we removed a number of low-activity meteor showers from our list. We removed showers if they had either few detections in the literature and/or non-detections in recent surveys or were removed from the IAU meteor shower list. The removed showers (and their common abbreviations) include the ω Scorpiids (OSC), ϵ Geminids (EGE or Eps), Comae Berenicids (COM or CBe), μ Virginids (DLI or mVi), α Centaurids (ACE), o Centaurids (oCe), γ Velids (GVE), δ Cancrids (DCA), α Carinids (aCa), δ Leonids (DLE), δ Pavonids (DPA), τ Cetids (TCT or Cet), τ Aquariids (TAQ), o Cygnids (OCY), Southern ι Aquariids (SIA or iAZ), Northern ι Aquariids (NIA or iAN), Northern δ Aquariids (NDA or dAN), γ Doradids (GDO), κ Aquariids (KAQ), Piscids (PSC or Pis), ζ Puppids (ZPU), α Monocerotids (AMO), χ Orionids (XOR or cOr), and Phoenicids (PHO).

Tables 2 and 3 provide the parameters for our standard shower list; this list reflects typical activity for each shower. Each year, we adjust those showers that are predicted to show unusual activity. For instance, the 2014 shower forecast included the May Camelopardalids, a new meteor shower that was predicted[1] to make its first appearance that year [21, 22, 23]. In 2016, the Perseids were predicted to reach approximately twice their usual rates and to exhibit multiple peaks in activity[2]; again, these predictions were incorporated into the 2016 annual shower forecast.

4. APPLICATION TO RISK ASSESSMENTS

The outputs of the meteor shower forecast are designed to support quick risk assessments for a spacecraft in low Earth orbit: all calculations are done at an altitude of 400

[1] http://www.imo.net/potentially-big-meteor-outburst-of-209p-meteors-on-may-24-2014/

[2] http://www.imo.net/perseids-2016-the-best-in-years/

km above the Earth's surface. We provide fluxes, fluences, and flux enhancement factors for the worst-case scenario in which a spacecraft surface directly faces a meteor shower radiant with no planetary shielding. Because hypervelocity impact damage is more closely related to kinetic energy than mass, our values are all kinetic-energy-limited. Table 1 provides the particles sizes and masses that correspond to our limiting kinetic energies for a particle velocity of 20 km s^{-1}.

Figs. 6-9 provide sample outputs from a meteor shower forecast that corresponds to typical annual meteor shower activity. Fig. 6 shows the zenithal hourly rate over the course of the year; while ZHR is not a useful quantity for risk assessments, it does illustrate how visual meteor rates vary with time. Fig. 7 presents the shower flux, which is more applicable to risk assessments. Fig. 7 also includes a horizontal line marking the time-averaged total meteoroid flux at 400 km altitude. Note that at smaller particle sizes, both the shower flux and total flux are larger, but showers contribute a smaller fraction. At the largest sizes, the flux is much lower, but showers are relatively more significant. The particle size at which showers constitute half of the total flux is larger than those modeled here: 10.5 g at 20 km s^{-1}, or 2.1 MJ (503 g TNT equivalent). For a density of 1000 kg m^{-3}, this corresponds to a particle diameter of 2.7 cm.

Fig. 8 presents the meteoroid fluence as a function of time. In this case, the fluence corresponds to the integral of the flux over a 7-hour period. We compute 7-hour fluences for our annual forecast, but provide custom forecasts in which the integration period can be specified by the customer. Finally, Fig. 9 shows the flux enhancement produced by showers over the course of the year. We report the flux enhancement on a surface facing the meteor shower; the contribution of meteor showers to the environment in general is one-fourth as large.

Our forecast enables quick assessments of the additional impact risk posed by a meteor shower. It does not contain detailed speed and directionality information like that provided by MEM [1, 2]. However, we do provide radiants for showers with high fluxes as part of our annual forecast. If a quick assessment using the forecasted shower flux enhancement indicates that the risk may be close to the acceptable threshold, further analysis should be done. This analysis should include the calculation of the aberrated radiant (taking gravitational focusing and the spacecraft's velocity vector into account), the total area presented to this aberrated radiant, and the angle(s) of impact onto that surface. The gravitational focusing and shielding factors we have used here are averaged over a sphere with a radius of $R_{\oplus} + 400$ km; however, gravitational focusing and shielding can exceed this average at some points on this sphere [7], and this, too, should be taken into account if the initial risk assessment is concerning.

We make one final, cautionary note regarding the use of these shower fluxes. We have endeavored to provide a worst-case scenario for the increase in particle *flux*. However, the width and depth of an impact crater can also depend on the impact angle. Thus, if a spacecraft surface faces the shower radiant, and the ballistic limit equation relevant to that surface predicts greater damage when the impact is normal (as in the modified Cour-Palais BLE for aluminum, [18]), the risk could be elevated by an even greater factor than the forecast is able to describe.

ACKNOWLEDGMENTS

This work was supported in part by NASA Cooperative Agreement NNX11AB76A and by the Natural Sciences and Engineering Research Council of Canada.

REFERENCES

1. McNamara H., Jones J., Kauffman B., et al., (2004). Meteoroid Engineering Model (MEM): A Meteoroid Model For The Inner Solar System, *Earth Moon and Planets*, **95**, 123–139.
2. Moorhead A., Koehler H., Cooke W., (2015). NASA Meteoroid Engineering Model Release 2.0, NASA/TM-2015-218214.
3. Dikarev V., Grün E., Baggaley J., et al., (2005). The new ESA meteoroid model, *Advances in Space Research*, **35**, 1282–1289.
4. Kronk G., (2014). *Meteor Showers*, Springer.
5. Moser D., Cooke W., (2004). MSFC Stream Model Preliminary Results: Modeling Recent Leonid and Perseid Encounters, *Earth Moon and Planets*, **95**, 141–153.
6. Moser D., Cooke W., (2008). Updates to the MSFC Meteoroid Stream Model, *Earth Moon and Planets*, **102**, 285–291.
7. Peterson G., (1999). *Dynamics of Meteor Outbursts and Satellite Mitigation Strategies*, The Aerospace Press, AIAA.
8. Jenniskens P., (1994). Meteor stream activity I. The annual streams, *Astronomy and Astrophysics*, **287**, 990–1013.
9. Jones J., Brown P., Ellis K., et al., (2005). The Canadian Meteor Orbit Radar: system overview and preliminary results, *Planetary & Space Science*, **53**, 413–421.
10. Campbell-Brown M., Jones J., (2006). Annual variation of sporadic radar meteor rates, *MNRAS*, **367**, 709–716.
11. Koschack R., Rendtel J., (1990). Determination of spatial number density and mass index from visual meteor observations (II), *WGN*, **18**, 119–140.
12. Verniani F., (1973). An Analysis of the Physical Parameters of 5759 Faint Radio Meteors, *Journal of Geophysical Research*, **78**, 8429–8462.

Table 2. Forecasting parameters for 11 meteor showers for which we obtained improved characterizations of the activity profile. Our improvements take the form of updated measurements of the peak time λ_0 and shape parameters B_p and B_m; new values appear in blue and previous values appear in red. In many cases, we have updated the shower name and corresponding three-letter code to comport with the International Astronomical Union's meteor shower list. Finally, we include peak zenithal hourly rate (ZHR_0), the shower's velocity at the top of the atmosphere ($v_{100\,\mathrm{km}}$), and the population index (r).

code	shower name	λ_0	B_p	B_m	ZHR_0	$v_{100\,\mathrm{km}}$	r
LYR	April Lyrids	~~32.32~~ 33.15	~~0.22~~ 1.229	~~0.22~~ 4.620	18	49	2.1
~~eAq~~ ETA	η Aquariids	~~45.5~~ 46.0	~~0.08~~ 0.125	~~0.08~~ 0.079	60	66	2.4
ZPE	ζ Perseids	~~78.6~~ 72.36	~~0.1~~ 0.028	~~0.1~~ 0.028	20	29	2.7
ARI	Daytime Arietids	~~76.8~~ 79.72	~~0.10~~ 0.065	~~0.10~~ 0.055	60	39	2.7
~~dAZ~~ SDA	~~Delta Aquarids South~~ Southern δ Aquariids	~~127.0~~ 124.93	~~0.091~~ 0.109	~~0.091~~ 0.071	20	42	3.2
CAP	Capricornids	~~127.0~~ 125.48	~~0.041~~ 0.059	~~0.041~~ 0.091	4	25	2.5
~~Sex~~ DSX	Daytime Sextantids	~~184.3~~ 189.44	~~0.1~~ 0.063	~~0.1~~ 0.167	5	32	2.7
ORI	Orionids	~~207.9~~ 209.18	0.12	~~0.12~~ 0.119	23	66	2.5
GEM	~~Geminids (peak)~~ ~~Geminids (base)~~ Geminids	~~262.2~~ ~~262.2~~ 262.23	~~0.590~~ ~~0.090~~ 0.150	~~0.81~~ ~~0.31~~ 0.462	~~100~~ ~~18~~ 118	35	2.6
URS	~~Ursids (peak)~~ ~~Ursids (base)~~ Ursids	~~270.7~~ ~~270.7~~ 270.96	~~0.900~~ ~~0.080~~ 2.292	~~0.900~~ ~~0.20~~ 1.258	~~10~~ ~~2~~ 12	33	3.0
QUA	~~Quadrantids (peak)~~ ~~Quadrantids (base)~~ Quadrantids	~~283.16~~ ~~283.16~~ 283.58	~~2.500~~ ~~0.370~~ 0.865	~~2.500~~ ~~0.45~~ 0.827	~~100~~ ~~20~~ 120	41	2.1

13. Grün E., Zook H., Fechtig H., Giese R., (1985). Collisional balance of the meteoritic complex, *Icarus*, **62**, 244–272.
14. Brown P., Jones J., Weryk R., Campbell-Brown M., (2004). The Velocity Distribution of Meteoroids at the Earth as Measured by the Canadian Meteor Orbit Radar (CMOR), *Earth Moon and Planets*, **95**, 617–626.
15. Moorhead A., Brown P., Campbell-Brown M., et al., (2017). Fully correcting the meteor speed distribution for radar observing biases, *Planetary & Space Science*, accepted.
16. Rendtel J., (2006). Visual Sporadic Meteor Rates, *WGN*, **34**, 71–76.
17. Rendtel J., (2007). Sporadic meteors, In *Proceedings of the International Meteor Conference, 25th IMC, Roden, Netherlands, 2006*, 99–103.
18. Hayashida K., Robinson J., (1991). Single wall penetration equations, NASA/TM-103565.
19. Kessler D., (1972). A Guide to Using Meteoroid-environment Models for Experiment and Spacecraft Design Applications, NASA/TN-D-6596.
20. Smith R., (1994). Natural Orbital Environment Guidelines for Use in Aerospace Vehicle Development, NASA/TM-4527.
21. Jenniskens P., (2006). *Meteor Showers and their Parent Comets*, Cambridge University Press.
22. Jenniskens P., (2014). Camelopardalids (IAU#451) from comet 209P/LINEAR, *WGN*, **42**, 98–105.
23. Ye Q., Wiegert P., (2014). Will comet 209P/LINEAR generate the next meteor storm?, *MNRAS*, **437** 3283–3287.

Table 3. Forecasting parameters for 17 meteor showers for which our activity profile parameters (λ_0, B_p, and B_m) remained unchanged. However, we have in some cases updated the shower name and corresponding three-letter code to comport with the International Astronomical Union's meteor shower list. Finally, we include peak zenithal hourly rate (ZHR_0), the shower's velocity at the top of the atmosphere ($v_{100\,km}$), and the population index (r).

code	shower name	λ_0	B+	B-	ZHR_0	$v_{100\,km}$	r
~~Sag~~ SSG	~~Gamma Sagitarids~~ Southern μ Sagittariids	88.5	0.037	0.037	2	29	2.9
BTA	Daytime β Taurids	96.7	0.100	0.100	10	29	2.7
~~uPh~~ PHE	~~Nu~~ July Phoenicids	110.5	0.25	0.25	5	48	3.0
PAU	~~Pisces Australids~~ (peak) Piscis Austrinids (base)	123.7	0.4 0.03	0.4 0.1	2 1	42	3.2
PER	Perseids (peak) (base)	140.05	0.35 0.05	0.35 0.092	80 23	61	2.6
~~kCy~~ KCG	κ Cygnids	145.0	0.069	0.069	3	27	3.0
AUR	Aurigids	158.6	0.190	0.190	9	66	2.6
SPE	September ϵ Perseids	166.7	0.193	0.193	5	64	2.9
DRA	Draconids	195.438	7.225	7.225	2	20	2.6
LMI	Leo Minorids	206.14	0.093	0.079	2	61	2.7
~~TaZ~~ STA	Southern Taurids	223.0	0.026	0.026	5	27	2.3
~~TaN~~ NTA	Northern Taurids	230.0	0.026	0.026	5	29	2.3
LEO	Leonids (peak) (base)	235.27 234.4	0.55 0.025	0.55 0.15	20 4	71	2.9
PUV	Puppids/Velids	255.0	0.034	0.034	10	40	2.9
MON	December Monocerotids	257.0	0.250	0.250	3	42	3.0
~~sHy~~ HYD	σ Hydrids	260.0	0.100	0.100	2	58	3.0
GNO	γ Normids	352.3	0.19	0.19	8	56	2.4

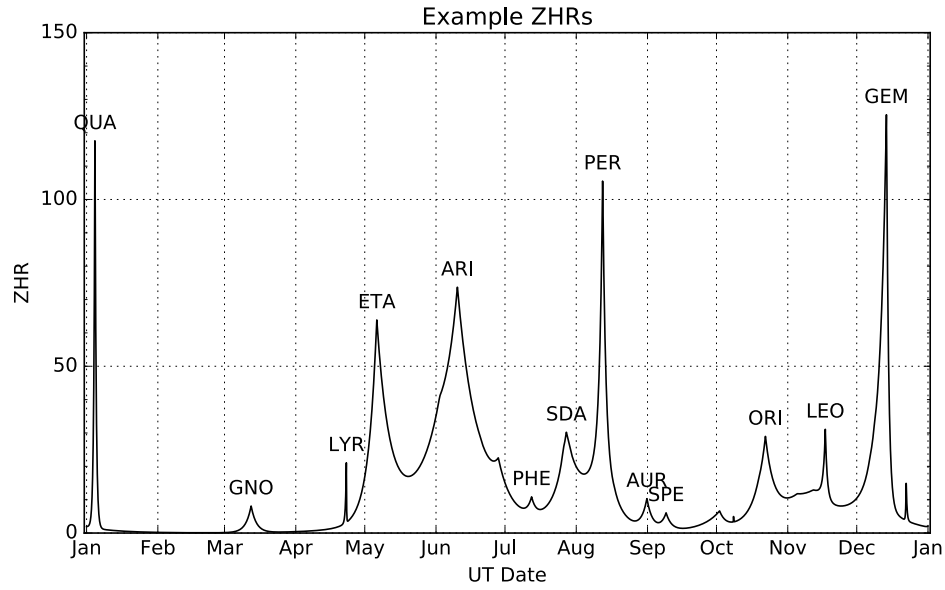

Figure 6. MEO annual meteor shower forecast sample output. This plot shows the total zenithal hourly rate (ZHR) due to meteor showers over the course of one year. Peaks corresponding to major meteor showers are labeled with the shower code.

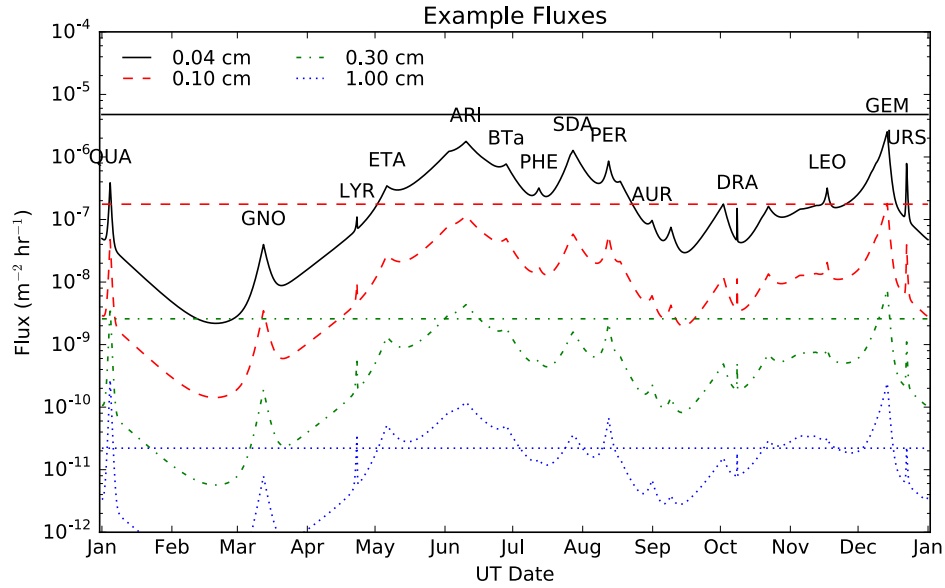

Figure 7. MEO annual meteor shower forecast sample output. This plot shows the total particle flux due to meteor showers over the course of one year for four particle energies (see Table 1). Peaks corresponding to major meteor showers are labeled with the shower code. The total flux (sporadic and shower combined) corresponding to each particle energy is also shown as a horizontal line. Note that for small particle sizes, meteor showers do not exceed the average flux, while at large sizes, many showers exceed the average. A similar plot is presented in Fig. 5.2 of [7].

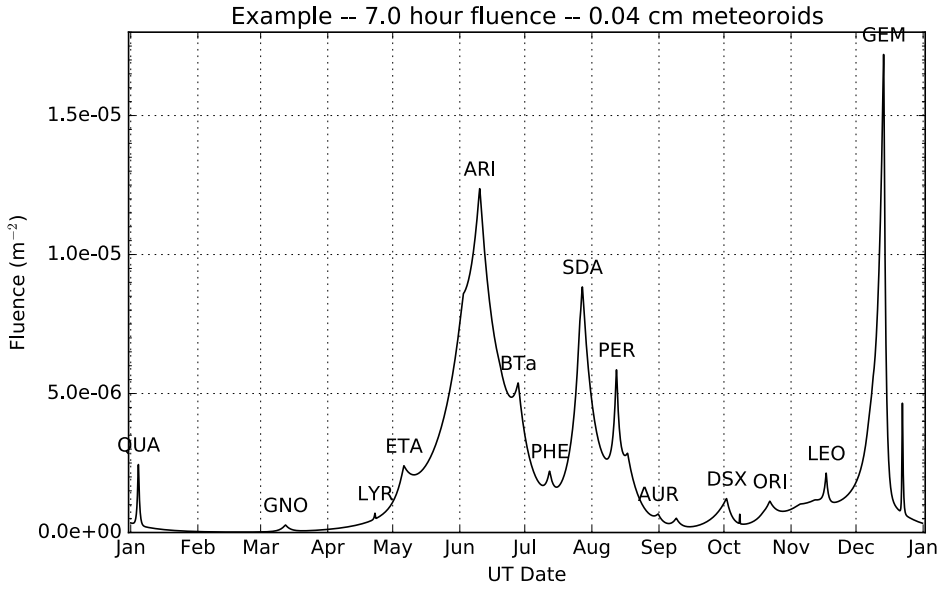

Figure 8. MEO annual meteor shower forecast sample output. This plot shows the 7-hour particle fluence (i.e., the flux integrated over a 7-hour period) due to meteor showers over the course of one year for the smallest reference particle size. Peaks corresponding to major meteor showers are labeled with the shower code.

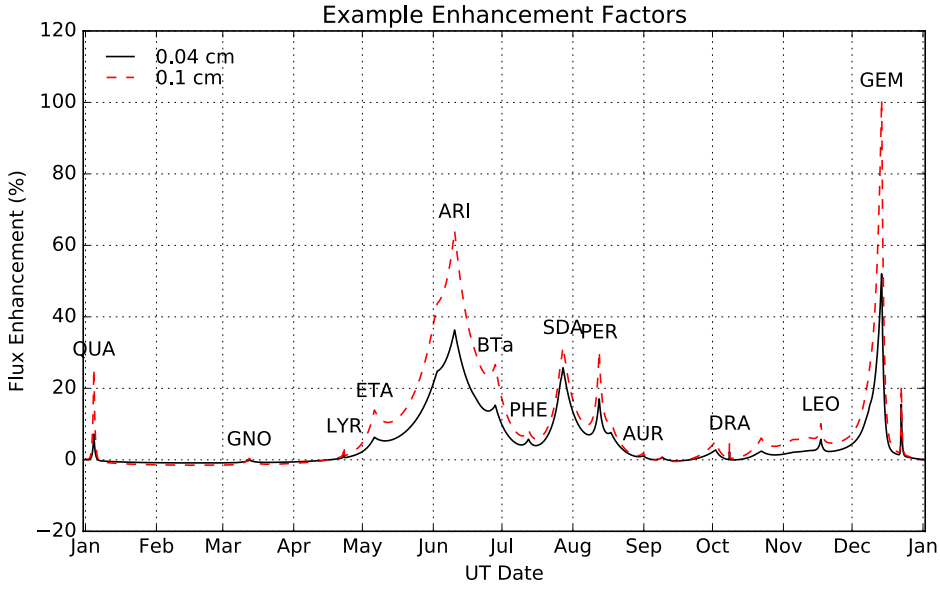

Figure 9. MEO annual meteor shower forecast sample output. This plot shows the enhancement of the total flux due to meteor showers for the smallest two reference particle sizes. Peaks corresponding to major meteor showers are labeled with the shower code. Fluxes, fluences, and enhancement factors assume that the spacecraft surface in question is oriented to face the shower radiant, maximizing the intercepted flux.